

Curvature Mapping Method: Mapping Lorentz Force in Orion A

Mengke Zhao^{1,2,3}, Guang-Xing Li², and Keping Qiu^{1,3}

¹ School of Astronomy and Space Science, Nanjing University, 163 Xianlin Avenue, Nanjing 210023, PR China

² South-Western Institute for Astronomy Research, Yunnan University, Kunming 650091, People's Republic of China e-mail: gxli@ynu.edu.cn

³ Key Laboratory of Modern Astronomy and Astrophysics (Nanjing University), Ministry of Education, Nanjing 210023, Jiangsu, PR China e-mail: kpqiu@nju.edu.cn

October 2, 2025

ABSTRACT

Magnetic force is a fundamental force in nature. Although widely believed to be important in counterbalancing against collapse in star formation, a clear evaluation of the role of the magnetic field in star formation remains hard to achieve. Past research attempts to evaluate the importance of magnetic forces using diagnostics such as the mass-to-flux ratio, which measures its strength but not how it functions. Since star formation is a complex process and the observed regions have complex structures, mapping the importance of the magnetic field is necessary. We propose a new technique, the *Curvature Mapping Method*, to evaluate the role of the 2D projected magnetic force by generating maps of the magnetic force derived from polarization observations. This method offers a clear visualization of the contribution of magnetic forces within a region. Its accuracy has been verified in MHD simulations, demonstrating reliable results in most cases. We apply the method to the star formation region of Orion A and provide the first quantitative result where the magnetic force arising from the hourglass magnetic field structure provides support against gravity, which the average Lorentz force is around $3 \times 10^{-26} \text{ G}^2 \text{ cm}^{-1}$. The method effectively uses information contained in polarization maps and can be applied to data from surveys to understand the role of the B-field.

Key words. Stars: formation – ISM: magnetic fields – ISM: clouds – ISM: molecules

1. Introduction

The magnetic field plays an important role in star formation (Larson 1981; McKee & Ostriker 2007; Li 2021), whose role in the star formation process is not entirely understood (Crutcher 2012; Li 2021; Pattle et al. 2023). Polarization observation (Planck Collaboration et al. 2016; Ward-Thompson et al. 2017; Harper et al. 2018) is the main magnetic field tracer, which can constrain the magnetic field morphology in the plane of the sky (POS). Large radio arrays, such as SMA, and ALMA, provide high-resolution dust polarization data to study magnetic fields of the interstellar medium (ISM) in star formation (Liu et al. 2020, 2024). The next stage is to analyze the information in these data sets to understand physics. The Davis-Chandrasekhar-Fermi (DCF; Davis 1951; Chandrasekhar & Fermi 1953) method is the most commonly used method, where the magnetic field strength is estimated through the dispersion of the polarization angle. The method is based on the assumption that the field lines are straight where the angle dispersion of the field lines is caused by turbulence, and this angle dispersion can be estimated using the dispersion of the polarization angle. However, in many cases, the magnetic field exhibits large-scale coherent structures where the assumption of almost-strain fields as required in the DCF breaks down. The question of how to analyze these data sets becomes an urgent one.

When the field lines are regular, the force is different from assumed in the DCF, where the field line becomes perturbed not to account for the turbulent pressure, but to counterbalance against gravity. In fact, those pinched magnetic field structures are usu-

ally interpreted as a balance between magnetic force and gravity in observations (Li et al. 2015; Pattle et al. 2017; Arzoumanian et al. 2021). Following this reasoning, Li et al. 2015 used this force balance to estimate the magnetic field strength by the balance between gravity and the Lorentz force. However, previous studies (Schleuning 1998; Qiu et al. 2014; Li et al. 2015) only applied this method to some particular cases. We argue that this argument is general and can estimate the Lorentz force in a much larger variety of simulations compared to Li et al. 2015. In this paper, we make the working assumption that the 2D magnetic field, as traced by e.g. the dust polarization observations, reflects the projection of the 3D magnetic field, through which the projected component of the magnetic force on the plane of sky can be estimated through the equation

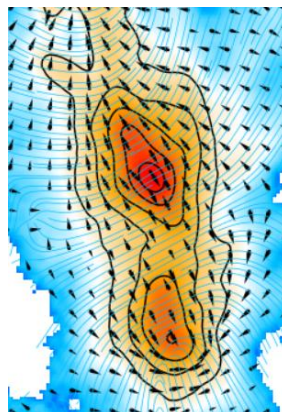
$$f_{L,POS} \approx \Omega f_{i,2D} = \frac{\Omega}{\mu_0} B^2 \cdot \kappa, \quad (1)$$

where the B and κ are the strength (scalar) and curvature (vector) of magnetic field, the Ω is a modified factor. This approach involves several underlying assumptions: First, the Lorentz force is comparable to the magnetic tension ($f_L \approx f_t$). Second, the 2D Lorentz force measured in our method reflects the 2D projected component of the 3D Lorentz force. As the discussion of the paper unfolds, one should see that both assumptions hold to some reasonable accuracy. Thus, one can estimate the behavior of the magnetic force using the dust polarization observations, which opens up new approach to the direct analysis of the effect of the magnetic force in the interstellar gas.

Curvature Mapping Method

Lorentz Force: **B-field strength** + **Curvature(feature)**

Map of Lorentz force $f_L \approx \Omega f_t = \frac{\Omega}{\mu_0} \mathbf{B}^2 \cdot \boldsymbol{\kappa}$



The spatially resolved directional information is complementary to B-field strength estimated from e.g. Zeeman and DCF.

Lorentz Force (vector)
B-field feature (line)

Fig. 1. Curvature Mapping method: mapping the Lorentz force in molecular clouds. Magnetic field strength and the curvature of the field lines combined to derive the Lorentz force. Previous studies estimate magnetic field strength using Zeeman splitting or the DCF method. In comparison, the Curvature Mapping Method can provide spatially resolved maps of the magnetic force.

2. Curvature Mapping Method

2.1. Magnetic tension comparable to Lorentz force

The Lorentz force is defined as the force acting on moving charged particles in an electromagnetic field and is related to the magnetic field \mathbf{B} and current density \mathbf{J} in plasma:

$$f_L = \mathbf{J} \times \mathbf{B}. \quad (2)$$

Using Ampère's law ($\mathbf{J} = (\nabla \times \mathbf{B})/\mu_0$), the Lorentz force can be expressed in terms of the magnetic field as:

$$f_L = \frac{1}{\mu_0} (\nabla \times \mathbf{B}) \times \mathbf{B} = \frac{(\mathbf{B} \cdot \nabla) \mathbf{B}}{\mu_0} - \nabla \left(\frac{\mathbf{B}^2}{2\mu_0} \right), \quad (3)$$

where the first term represents magnetic tension and the second term represents magnetic pressure.

The magnetic tension is similar to Lorentz force. Past studies have shown that the energy cascade of MHD turbulence is suppressed by magnetic tension (Grete et al. 2021), suggesting that magnetic tension plays a significant role in the Lorentz force. Comparisons between magnetic tension and the Lorentz force in MHD numerical simulations using the Enzo code (Collins et al. 2012; Burkhart et al. 2015) reveal that the magnetic tension closely resembles the Lorentz force in both magnitude and orientation (details provided in Appendix B). Assuming that magnetic tension approximates the Lorentz force, we can estimate the Lorentz force as:

$$f_L \approx \Omega_1 f_t = \frac{\Omega_1}{\mu_0} (\mathbf{B} \cdot \nabla) \mathbf{B} = \Omega_1 \frac{\mathbf{B}^2}{\mu_0} (\mathbf{b} \cdot \nabla) \mathbf{b} = \Omega_1 \frac{\mathbf{B}^2}{\mu_0} \cdot \boldsymbol{\kappa}, \quad (4)$$

where \mathbf{B} represents the magnetic field strength, \mathbf{b} is the unit vector of the magnetic field, and $\boldsymbol{\kappa}$ is the magnetic field curvature vector derived from the magnetic field morphology. Since the magnetic tension, pressure and Lorentz force are similar in the simulation (see Ap. B), the Ω_1 as a weighting factor represents the effect of the magnetic pressure in the Lorentz force. This assumption allows the Lorentz force to be decomposed into two components: a scalar parameter representing magnetic field strength and a vector parameter derived from the magnetic field morphology.

2.2. Adapt observation: from 3D to 2D

The observation of the magnetic field, different from data of the MHD simulation, only has the 2D magnetic field orientation (eg. polarization (Pattle et al. 2017; Chuss et al. 2019; Planck Collaboration et al. 2020a)) in the plane of sky (POS) and the estimation of total magnetic strength (eg. DCF method (Pattle et al. 2023), Zeeman splitting (Crutcher et al. 2010)). Thus, we assume the 2D magnetic tension is close to the Projected component of Lorentz force to measure the projected Lorentz force on POS. According to Eq. 4, this projected Lorentz force depends on the magnetic curvature on POS.

2D curvature vector can be credibly calculated by POS magnetic field orientation in most cases. Curvature is the key parameter of our method, which is calculated by the unit vector of the magnetic field. The POS unit vector can be obtained from magnetic field orientation ϕ , the x, y components as the $\cos\phi$ and $\sin\phi$. For tracing the projected component of Lorentz force, the magnetic field orientation in POS observed by dust polarization should present the main structure of the 3D magnetic field. When the magnetic field vector along the LOS is less than that of the POS, the POS structure could be the main structure of the whole field, and the offset angle between the LOS vector and the POS plane is less than 45° . If the magnetic field vector is randomly distributed (Crutcher et al. 2004), the probability of the offset angle between the LOS vector and the POS plane being less than 45° is around 71% according to the probability density ($p(\theta) = 0.5\sin\theta$). The POS magnetic field structure could present the main magnetic field morphology to calculate the projected curvature and Lorentz force in most cases. The components of the magnetic curvature vector $\boldsymbol{\kappa}$ can then be calculated as:

$$\kappa_x = \cos\phi_B \frac{\partial}{\partial x} \cos\phi_B + \sin\phi_B \frac{\partial}{\partial y} \cos\phi_B, \quad (5)$$

$$\kappa_y = \cos\phi_B \frac{\partial}{\partial x} \sin\phi_B + \sin\phi_B \frac{\partial}{\partial y} \sin\phi_B, \quad (6)$$

$$\boldsymbol{\kappa} = \kappa_x \mathbf{i} + \kappa_y \mathbf{j}, \quad (7)$$

where κ_x and κ_y are the curvature components along the x- and y-axes.

2.3. Tracing the Projected Lorentz force on POS

The projected component of Lorentz force in the plane of the sky (POS) can be measured using the POS magnetic field morphology and magnetic field strength (see Fig. 1). For easy application in observation, the Projected Lorentz force is calculated by the magnetic curvature (2D vector) and total magnetic field strength (scaler) in 2D plane

$$f_{L,\text{projected}} \approx C f_{t,2D} = C \frac{\Omega_1}{\mu_0} B_{\text{POS}}^2 \boldsymbol{\kappa} = \frac{\Omega}{\mu_0} B_{\text{tot}}^2 \boldsymbol{\kappa}, \quad (8)$$

where Ω is a modified factor including projection effects of the Lorentz force, the effect of magnetic pressure, typically ranging between 1 and 1.5 (detailed in Sect. 3.2).

The POS-projected Lorentz force thus depends on two primary physical parameters: the scalar term B_{tot} (magnetic field strength) and the vector term $\boldsymbol{\kappa}$ (magnetic field curvature). The curvature vector $\boldsymbol{\kappa}$ can be derived from magnetic field orientations, generally observable through dust polarization (Ward-Thompson et al. 2017; Planck Collaboration et al. 2020b). The total Magnetic field strength, B_{tot} , can be estimated using many methods such as Zeeman splitting (Crutcher et al. 2010), the DCF method (Davis 1951; Chandrasekhar & Fermi 1953; Crutcher et al. 2004), the ST method (Skalidis & Tassis 2021; Skalidis et al. 2021), and so on.

As advances in observations, the projected Lorentz force can be mapped as vectors in the POS, including both its strength and orientation. This technique, known as the *Curvature Mapping Method*, has the added advantage of resolving the Lorentz force orientation over the full range of 0 to 2π . Importantly, curvature is invariant under magnetic field vector direction, ensuring:

$$(\mathbf{b} \cdot \nabla) \mathbf{b} = (-\mathbf{b} \cdot \nabla) - \mathbf{b}. \quad (9)$$

Thus, the curvature orientation spans 0 to 2π , unaffected by the polarization-based magnetic field orientation (0 to π) observed in the POS. Caution is required in its application under certain conditions, such as when the magnetic field structure is perfectly straight without curved or when magnetic pressure effects dominate significantly, since the assumptions of this method may be less valid in these cases, although these scenarios could be un-frequent (Planck Collaboration et al. 2016; Grete et al. 2021). In most cases, the Curvature Mapping Method effectively measures the projected Lorentz force using the POS magnetic field morphology. The verification of this method is presented in the next section.

3. Verify the Accuracy of the Curvature Mapping Method in Simulation

To verify the accuracy of the curvature mapping method in tracing the POS projected component of Lorentz force, we compare the Lorentz force calculated using the curvature mapping method (referred to as the pseudo Lorentz force) with the projected component of the 3D Lorentz force on the 2D plane (referred to as the projected Lorentz force).

The components of the Lorentz force along the x-, y-, and z-axes are given by:

$$f_L = f_{L,x} \mathbf{i} + f_{L,y} \mathbf{j} + f_{L,z} \mathbf{k} = \frac{1}{\mu_0} (\nabla \times \mathbf{B}) \times \mathbf{B}, \quad (10)$$

where the magnetic field vector is $\mathbf{B} = B_x \mathbf{i} + B_y \mathbf{j} + B_z \mathbf{k}$. The projected Lorentz force in the x-y plane is:

$$f_{L,\text{projected}} = f_{L,x} \mathbf{i} + f_{L,y} \mathbf{j}. \quad (11)$$

The pseudo Lorentz force derived using the curvature mapping method is computed from the unit vectors of the magnetic field in the x-y plane and the total magnetic field strength, close to the usage scenario:

$$f_{\text{CMM}} = \frac{B_{\text{tot}}^2}{\mu_0} (\mathbf{b}_{x,y} \cdot \nabla) \mathbf{b}_{x,y} = \frac{B_{\text{tot}}^2}{\mu_0} \boldsymbol{\kappa}_{x,y}, \quad (12)$$

where \mathbf{b}_x and \mathbf{b}_y are the unit vectors defined as $\mathbf{B}_x / \sqrt{B_x^2 + B_y^2}$ and $\mathbf{B}_y / \sqrt{B_x^2 + B_y^2}$, respectively, in each x-y plane, and $B_{\text{tot}} = \sqrt{B_x^2 + B_y^2 + B_z^2}$ is the total magnetic field strength. The modified factor Ω is temporarily assumed to be 1. The x and y components of the pseudo Lorentz force are:

$$f_{x,\text{CMM}} = B_{\text{tot}}^2 \left(b_x \frac{\partial b_x}{\partial x} + b_y \frac{\partial b_x}{\partial y} \right), \quad (13)$$

$$f_{y,\text{CMM}} = B_{\text{tot}}^2 \left(b_x \frac{\partial b_y}{\partial x} + b_y \frac{\partial b_y}{\partial y} \right). \quad (14)$$

In this way, we simulate random observational perspectives using MHD simulations with 256^3 data points to verify the accuracy of the Curvature Mapping Method in determining both the orientation and strength of the Lorentz force.

3.1. Comparison of Orientations

To evaluate the accuracy of the curvature mapping method, we compare the orientations of the pseudo Lorentz force and the projected Lorentz force. The offset angle between them in the x-y plane is:

$$\theta_{f_{L,\text{projected}}, f_{\text{CMM}}} = \tan^{-1} \left(\frac{f_{L,y}}{f_{L,x}} \right) - \tan^{-1} \left(\frac{f_{y,\text{CMM}}}{f_{x,\text{CMM}}} \right). \quad (15)$$

We analyzed the offset angles in each slice along the z-axis for three MHD simulations (weak, middle, and strong magnetic field states) to simulate the variety of visual angles observed in actual observations ($256 \times 256 \times 256$ points per simulation, see Fig. 2). As shown in Fig. 2, 40%, 50%, 50% of the points in weak, middle, and strong magnetic states ($\mathcal{M}_A \sim 0.3, 0.5, \text{ and } 1.3$, Zhao et al. 2024), exhibit parallel alignment ($\theta_{f_{L,\text{projected}}, f_{\text{CMM}}} \lesssim 30^\circ$), and 50%, 60%, 60% of these simulations show close to parallel alignment ($\theta_{f_{L,\text{projected}}, f_{\text{CMM}}} \lesssim 45^\circ$). This result demonstrates that the curvature mapping method effectively traces the orientation of the projected Lorentz force in the most cases.

3.2. Strength Modification of Projected Lorentz Force

The curvature mapping method estimates the 2D projected Lorentz force based on the POS magnetic field morphology and the total magnetic field strength. A modified factor Ω from projected effect is introduced to improve the accuracy:

$$\Omega = \frac{f_{L,\text{projected}}}{f_{\text{CMM}}} = \frac{\sqrt{f_{L,x}^2 + f_{L,y}^2}}{\sqrt{f_{x,\text{CMM}}^2 + f_{y,\text{CMM}}^2}}. \quad (16)$$

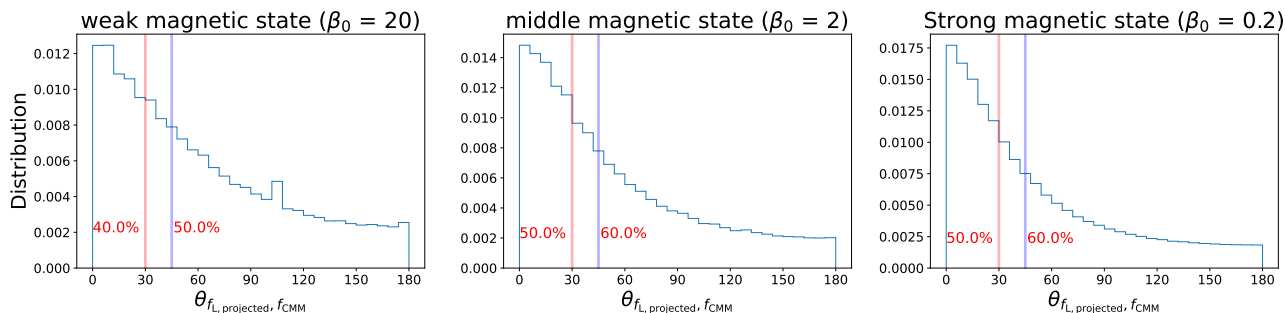


Fig. 2. Distribution of offset angle between pseudo Lorentz force and Projected Lorentz force in MHD simulations. The three panels present the distribution of offset angle between pseudo Lorentz force and Projected Lorentz force in weak, middle, and strong magnetic field states, respectively. The percentages of offset angle $< 30^\circ$ (parallel aligned) are around 40%, 50%, and 50% in weak, middle, and strong magnetic field states, respectively. That of offset angle $< 45^\circ$ (close to parallel) are around 50%, 60%, and 60% in weak, middle, and strong magnetic field states, respectively.

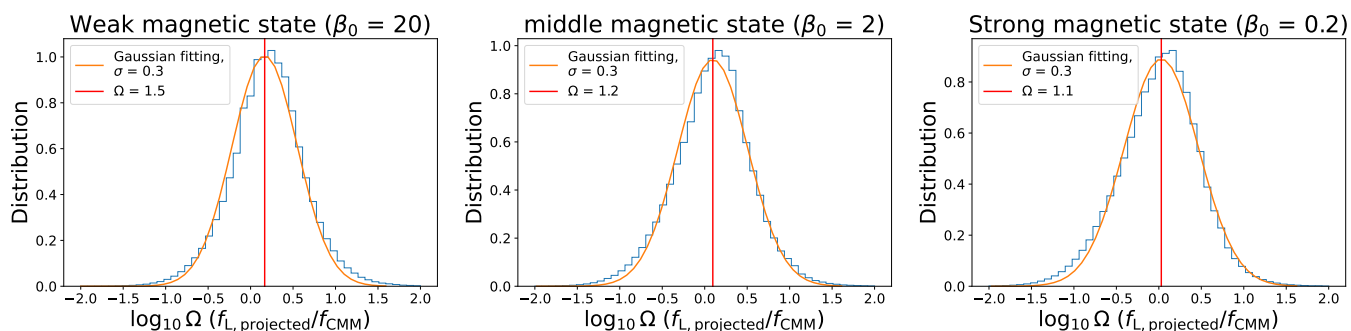


Fig. 3. Distribution of modified factors of curvature mapping method in various magnetic field states. The ratio between the projected Lorentz force and the pseudo Lorentz force presents the modified factor Ω of curvature mapping method. In three simulations (weak, middle, and strong magnetic state in left, middle, and right panel), the distribution of modified factor forms norm distributions, where the mean values are 1.5, 1.2, and 1.1 with the standard deviation around 0.3 at the log scale.

As shown in Fig. 3, the ratio $f_{L,\text{projected}}/f_{\text{CMM}}$ from simulations follows a nearly normal distribution, with a standard deviation of 0.3 orders of magnitude (around two times). Gaussian fitting yields peak values of 1.1, 1.2, and 1.5 for weak, middle, and strong magnetic field states, respectively. Thus, Ω ranges from 1.1 to 1.5.

Above all, the projected Lorentz force can be calculated by Curvature mapping method as:

$$f_{L,\text{CMM}} = \Omega \frac{B_{\text{tot}}^2}{\mu_0} \kappa, \quad (17)$$

where Ω is approximately 1.1 to 1.5, B_{tot} is the scalar term of total magnetic field strength, and κ is the vector term, magnetic curvature derived from the magnetic field structure. Therefore, we use the OMC-1 magnetic field with a classical 2D "hour-glass" structure (Pattle et al. 2017) as an example to show the application of the curvature mapping method.

4. Mapping Lorentz Force in Orion A

Orion A is a well-known massive star-forming region located approximately 400 pc away (Menten et al. 2007). Within this molecular cloud lies the OMC-1 region, featuring a distinctive pinched magnetic field structure (see Fig. 5), which is a hallmark of hourglass magnetic field configurations.

By applying the Curvature Mapping Method to magnetic field observations of OMC-1 (Falgarone et al. 2008; Pattle et al. 2017), we constructed a Lorentz force map as vector fields within the molecular cloud. The vector form of the projected Lorentz force is determined using the Curvature Mapping Method, which relies on both scalar term (magnetic field strength) and vector terms (magnetic curvature):

$$f_{\vec{L}} = \frac{\Omega}{\mu_0} B_{\text{tot}}^2 \kappa, \quad (18)$$

where the orientation of the projected Lorentz force is aligned with the direction of the magnetic curvature, and its strength is predominantly influenced by the magnitude of the magnetic field strength and the magnetic curvature.

With reliable magnetic field structures from observations, the magnetic curvature can be readily derived from observations (see Sect. 2). However, estimating magnetic field strength remains a significant observational challenge. To address this limitation, we propose two approaches for studying the Lorentz force from observations:

- Determination of the map of Lorentz force structure (orientation) and the size of magnetic curvature.
- Full vector mapping of the Lorentz force, encompassing both orientation and strength.

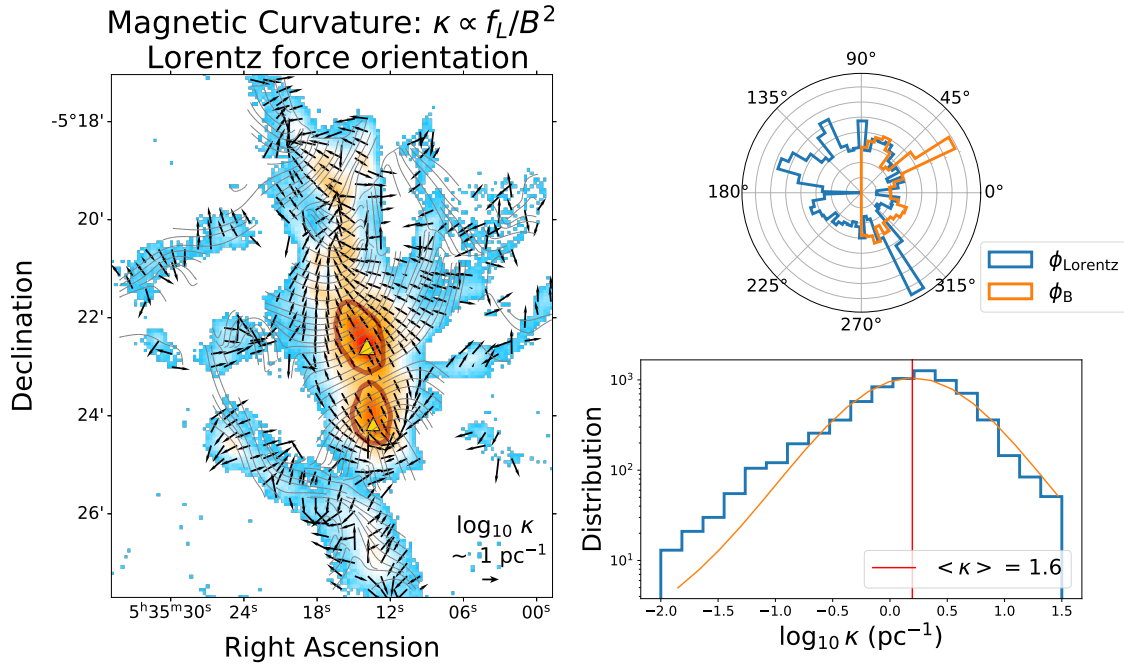


Fig. 4. Distribution of magnetic curvature and Lorentz force orientations. The left panel displays the magnetic curvature map (black arrows), where the arrow orientations represent the orientation of the Lorentz force. The background illustrates the $850\mu\text{m}$ continuum emission, while the streamlines depict the magnetic field structure derived from $850\mu\text{m}$ dust polarization observations. The contours show the column density as $10^{23.4} \text{ cm}^{-2}$ and the triangle markers display the position of clumps Orion-KL and Orion South. The top-right panel shows the orientation distributions of the Lorentz force (blue) and the magnetic field (orange). The Lorentz force orientation peaks at angles perpendicular to those of the magnetic field, indicating the expected orthogonality between the two. The bottom-right panel presents the distribution of magnetic curvature magnitudes. The orange line represents a Gaussian fit to the distribution, and the red line indicates the average curvature value ($\langle \kappa \rangle \sim 1.6 \text{ pc}^{-1}$).

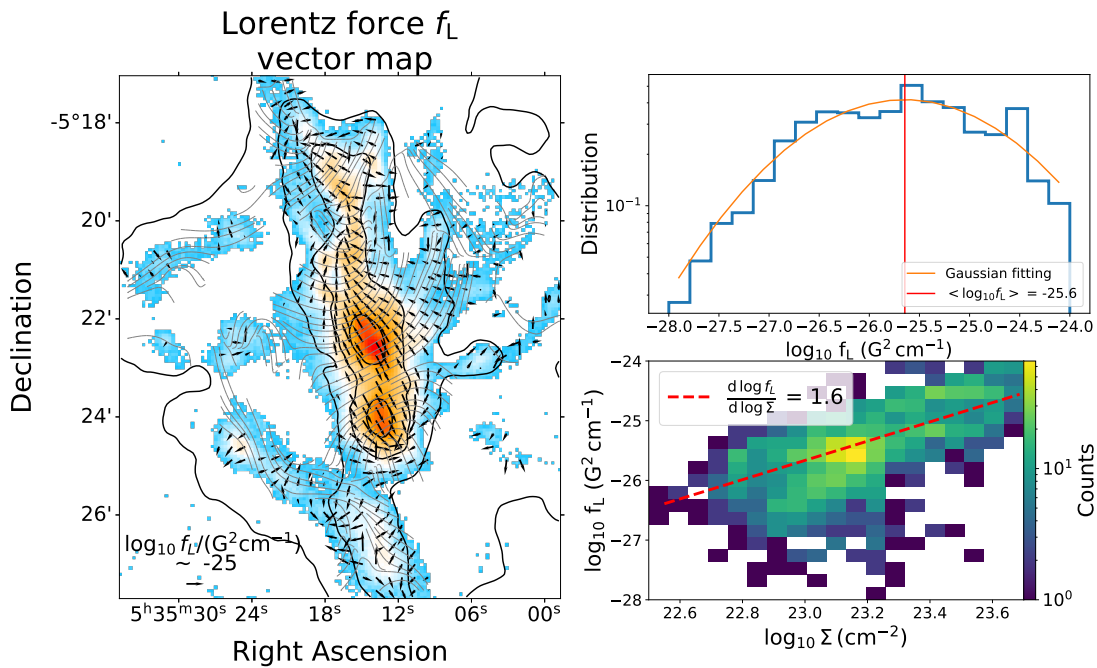


Fig. 5. Distribution of Lorentz force vector. The left panel displays the vector map of the Lorentz force (black arrows). The background illustrates the $850\mu\text{m}$ continuum emission, while the streamlines depict the magnetic field structure derived from $850\mu\text{m}$ dust polarization observations. Black contours show the H_2 column density from Herschel from 10^{22} to $10^{23.5} \text{ cm}^{-2}$ with step as $10^{0.5}$. The bottom-right panel presents the 2D histogram of Lorentz force and H_2 column density. The red dot line fits a 'power law' relation between Lorentz force and H_2 column density. The top-right pane presents the distribution of Lorentz force weighted by column density, due to the Lorentz force strength related to column density. The orange line represents a Gaussian fit to the distribution, and the red line indicates the average curvature value ($\langle f_L \rangle \sim 2.5 \times 10^{-26} \text{ G}^2 \text{ cm}^{-1}$).

4.1. Lorentz Force structure

The orientations and structure of Lorentz force can be traced by the orientation of magnetic curvature derived by magnetic field morphology. As Fig. 4 shows, the Lorentz force exhibits a structured, bipolar geometry in OMC-1 with an hourglass-shaped magnetic field. The observed Lorentz force distribution highlights localized regions of high curvature in the magnetic field, where the force vectors often diverge in opposing directions, forming a bipolar pattern. This structure suggests that the Lorentz force plays a critical role in regulating gas dynamics and counteracting gravitational collapse in these regions.

In the context of star formation, this interplay between Lorentz force and gravity is crucial. The Lorentz force in the hourglass-shaped magnetic field acts as a counterbalance to gravity, slowing down the collapse of gas and dust in molecular clouds (Galli & Shu 1993; Allen et al. 2003; Qiu et al. 2014). This magnetic support is particularly important in regions of high curvature, where the magnetic field's resistance to distortion is strongest. By buffering against gravitational collapse, the Lorentz force helps regulate the rate of star formation, preventing rapid and unregulated fragmentation of the cloud (Hacar et al. 2017).

The orientation of the force is theoretically perpendicular to its potential field. As Fig. 4 shows, the orientation of Lorentz force is perpendicular to the magnetic field both POS plane morphology and statistics polar space of orientations. By ensuring the magnetic field lines and the Lorentz force vectors are consistently orthogonal, we can be more confident in the robustness of the curvature mapping method used to derive the force structures in these regions.

4.2. Estimated magnetic field strength

Direct measurement of magnetic field strength in the interstellar medium (ISM) remains challenging. However, indirect methods, such as assuming force balance between magnetic and gravitational forces, provide viable estimates. As Fig. 4 shows, the Lorentz force in OMC-1, oriented along the filament body, supports against gravitational collapse (Hacar et al. 2017). By equating the Lorentz force to the self-gravity, the magnetic field strength can be estimated as:

$$f_L = \frac{\Omega}{\mu_0} B_{\text{tot}}^2 \langle \kappa \rangle = f_{\text{gravity}} \quad (19)$$

where the f_{gravity} is the volume density of gravity ($F_{\text{gravity}} = f_{\text{gravity}} \cdot \text{Volume}$, due to the projected Lorentz force as the volume density of magnetic force. We use a gravitational collapse region, OMC-1 (Hacar et al. 2017; Wu et al. 2024) as an example to estimate its magnetic field strength.

We apply this method to the star-forming region OMC-1, where Orion-KL and Orion-South (Fig. 4) are the dominant gravitational sources. Using column density maps ($N(\text{H}_2) > 10^{23.4} \text{ cm}^{-2}$, see Fig. 4), we derive clump masses M1 (Orion-KL) and M2 (Orion-South), separated by $L \approx 0.2 \text{ pc}$. The gravity is roughly computed as $F_{\text{gravity}} = GM_1 M_2 L^{-2}$.

Assuming force balance, the magnetic field strength is:

$$B_{\text{tot,L}} = \left(\frac{\mu_0}{\Omega \langle \kappa \rangle \text{volume}} F_{\text{gravity}} \right)^{\frac{1}{2}} = \left(\frac{\mu_0}{\Omega \langle \kappa \rangle} \frac{F_{\text{gravity}}}{L^3} \right)^{\frac{1}{2}} \quad (20)$$

The magnetic curvature κ in OMC-1 follows a Gaussian distribution with a mean value of 1.6 pc^{-1} (Fig. 4). This yields an estimated field strength around 0.5 mG , consistent with Zeeman splitting measurements ($\sim 0.7 \text{ mG}$, Crutcher et al. 2010) and

Davis-Chandrasekhar-Fermi (DCF) methods combined with autocorrelation function (ACF) analysis (0.6 mG ; Wu et al. 2024). The magnetic field strength can be estimated by magnetic curvature from curvature mapping method. Of course, magnetic curvature would have more applications, including estimating magnetic field strength.

4.3. Mapping vector of Lorentz force in OMC-1

If a reliable magnetic field strength distribution is available, the Lorentz force can be mapped in vector form (see Fig. 5). Using the ST method (Skalidis & Tassis 2021; Skalidis et al. 2021), the magnetic field strength distribution is derived based on density, non-thermal velocity dispersion, and the angular dispersion of the magnetic field orientation (details are shown in Fig. D).

By combining the distribution maps of magnetic field strength (B_{tot} ; see Fig. C.1) and magnetic curvature (κ ; see Fig. 4), the Lorentz force vectors can be calculated using the following expression:

$$f_L = \frac{\Omega}{\mu_0} B_{\text{tot}}^2 \kappa, \quad (21)$$

where the correction factor Ω is taken as 1.5. The resulting Lorentz force vector map is displayed in Fig. 5.

The orientation of the Lorentz force is dictated by the magnetic curvature, as discussed in Sect. 4.1. Fig. 4 shows that the Lorentz force is strongest in high-density regions, while it diminishes in low-density areas. The Lorentz force relates to the H_2 column density in OMC-1, presented as a power law distribution ($f_L \propto \Sigma^{1.6}$).

When weighted by column density, the probability density function (PDF) of the Lorentz force approximates a normal distribution. A Gaussian fit to the PDF reveals an average Lorentz force magnitude of approximately $2.5 \times 10^{-26} \text{ G}^2 \text{ cm}^{-1}$.

Above, the Curvature Mapping Method enables the determination of both the orientation of the Lorentz force and the magnetic curvature from reliable magnetic field observations. One of the applications is estimating the magnetic field strength of molecular clouds using the strength of magnetic curvature. Furthermore, when the spatial distribution of the magnetic field strength is reliably obtained, the method allows for the construction of a detailed vector map of the projected Lorentz force in the interstellar medium. In the future, the Curvature mapping method will develop more applications to study the magnetic field of the interstellar medium and star formation.

5. Conclusion

We propose a new technique, the Curvature Mapping Method, to plot the vector map of the projected Lorentz force in the interstellar medium on the plane of the sky. The method is based on the idea that the Lorentz force is closely related to magnetic tension, which depends on the morphology and strength of the magnetic field:

$$f_L = \frac{\Omega}{\mu_0} B_{\text{tot}}^2 \cdot \kappa,$$

where the magnetic field strength B_{tot} is the scalar term, the magnetic curvature κ is the vector term, and the modified factor Ω for the projected effect ranges from [1.1, 1.5]. The magnetic curvature, calculated from the magnetic field morphology, is a critical parameter of the Curvature Mapping Method and determines the orientation of the POS Lorentz force.

We test the accuracy of the Curvature Mapping Method to trace the projected Lorentz force using MHD simulations. In most cases (around 50%-60%), the orientation of Lorentz force measured by the Curvature Mapping Method is closely aligned with the projected component of the true Lorentz force. Its strength is also comparable to the real value of the 2D projected Lorentz force, with an error of approximately $10^{0.3}$ (~ two times).

Applying the Curvature Mapping Method to observations, there are three usage scenarios depending on the input parameters:

- Based on credible magnetic field morphology, such as from dust polarization, the Curvature Mapping Method can determine the magnetic curvature and orientation of the POS Lorentz force.
- Based on magnetic curvature from magnetic field morphology, the magnetic field strength can be estimated
- If a credible magnetic field strength map is obtained, the vector map of the Lorentz force can be derived.

We measure the Lorentz force in OMC-1, which exhibits an hourglass-shaped magnetic field structure. The Lorentz force morphology presents a bipolar structure and supports gravity. The average magnetic curvature in OMC-1 is approximately 1.6 pc^{-1} . Using the single magnetic field strength derived from Zeeman splitting ($\sim -720 \mu\text{G}$), the average strength of the Lorentz force is calculated as $3 \times 10^{-26} \text{ G}^2, \text{cm}^{-1}$. Using the magnetic curvature and the assumption of balance between Lorentz force and gravity, the magnetic field strength in OMC-1 is estimated as 0.5 mG , in agree with previous studies (Crutcher et al. 2010; Wu et al. 2024). As the column density increases, the Lorentz force grows larger ($f_L \propto \Sigma^{1.6}$). The weighted average Lorentz force is approximately $2.5 \times 10^{-26} \text{ G}^2, \text{cm}^{-1}$.

By effectively using the information in the polarization map, the Curvature Mapping Method provides direct insights into the role of B-field in star-forming regions and can be widely applied. Our spatially-resolved approach takes full advantage of the information in the map, leading to direction vision into the role of the magnetic field. With this unprecedented amount of polarization measurements gathered by modern instruments, by combining our results with other methods with spatial information, such as gravitational acceleration mapping (He et al. 2023), direct insights into the role of the magnetic field in regulating star formation can be obtained.

References

Allen, A., Shu, F. H., & Li, Z.-Y. 2003, *ApJ*, 599, 351
 Arzoumanian, D., Furuya, R. S., Hasegawa, T., et al. 2021, *aap*, 647, A78
 Burkhart, B., Appel, S. M., Bialy, S., et al. 2020, *apj*, 905, 14
 Burkhart, B., Collins, D. C., & Lazarian, A. 2015, *apj*, 808, 48
 Chandrasekhar, S. & Fermi, E. 1953, *apj*, 118, 113
 Chuss, D. T., Andersson, B. G., Bally, J., et al. 2019, *apj*, 872, 187
 Collins, D. C., Kritsuk, A. G., Padoan, P., et al. 2012, *apj*, 750, 13
 Collins, D. C., Xu, H., Norman, M. L., Li, H., & Li, S. 2010, *apjs*, 186, 308
 Crutcher, R. M. 2012, *araa*, 50, 29
 Crutcher, R. M., Nutter, D. J., Ward-Thompson, D., & Kirk, J. M. 2004, *apj*, 600, 279
 Crutcher, R. M., Wandelt, B., Heiles, C., Falgarone, E., & Troland, T. H. 2010, *apj*, 725, 466
 Davis, L. 1951, *Physical Review*, 81, 890
 Falgarone, E., Troland, T. H., Crutcher, R. M., & Paubert, G. 2008, *aap*, 487, 247
 Friesen, R. K., Pineda, J. E., co-PIs, et al. 2017, *ApJ*, 843, 63
 Galli, D. & Shu, F. H. 1993, *ApJ*, 417, 220
 Grete, P., O’Shea, B. W., & Beckwith, K. 2021, *ApJ*, 909, 148
 Griffin, M. J., Abergel, A., Abreu, A., et al. 2010, *aap*, 518, L3
 Hacar, A., Alves, J., Tafalla, M., & Goicoechea, J. R. 2017, *aap*, 602, L2

Harper, D. A., Runyan, M. C., Dowell, C. D., et al. 2018, *Journal of Astronomical Instrumentation*, 7, 1840008
 He, Z.-Z., Li, G.-X., & Burkert, A. 2023, *mnras*, 526, L20
 Houde, M., Hull, C. L. H., Plambeck, R. L., Vaillancourt, J. E., & Hildebrand, R. H. 2016, *ApJ*, 820, 38
 Houde, M., Vaillancourt, J. E., Hildebrand, R. H., Chitsazzadeh, S., & Kirby, L. 2009, *ApJ*, 706, 1504
 Larson, R. B. 1981, *mnras*, 194, 809
 Li, G.-X. 2022, *ApJS*, 259, 59
 Li, H.-B. 2021, *Galaxies*, 9, 41
 Li, H.-B., Yuen, K. H., Otto, F., et al. 2015, *nat*, 520, 518
 Liu, J., Zhang, Q., Lin, Y., et al. 2024, *arXiv e-prints*, arXiv:2403.03437
 Liu, J., Zhang, Q., Qiu, K., et al. 2020, *apj*, 895, 142
 McKee, C. F. & Ostriker, E. C. 2007, *araa*, 45, 565
 Menten, K. M., Reid, M. J., Forbrich, J., & Brunthaler, A. 2007, *A&A*, 474, 515
 Pattle, K., Fissel, L., Tahani, M., Liu, T., & Ntormousi, E. 2023, in *Astronomical Society of the Pacific Conference Series*, Vol. 534, *Protostars and Planets VII*, ed. S. Inutsuka, Y. Aikawa, T. Muto, K. Tomida, & M. Tamura, 193
 Pattle, K., Ward-Thompson, D., Berry, D., et al. 2017, *apj*, 846, 122
 Planck Collaboration, Ade, P. A. R., Aghanim, N., et al. 2016, *aap*, 586, A138
 Planck Collaboration, Aghanim, N., Akrami, Y., et al. 2020a, *aap*, 641, A12
 Planck Collaboration, Aghanim, N., Akrami, Y., et al. 2020b, *aap*, 641, A1
 Poglitsch, A., Waelkens, C., Geis, N., et al. 2010, *aap*, 518, L2
 Polychroni, D., Schisano, E., Elia, D., et al. 2013, *apjl*, 777, L33
 Qiu, K., Zhang, Q., Menten, K. M., et al. 2014, *ApJ*, 794, L18
 Roy, A., Martin, P. G., Polychroni, D., et al. 2013, *apj*, 763, 55
 Schleuning, D. A. 1998, *ApJ*, 493, 811
 Skalidis, R., Sternberg, J., Beattie, J. R., Pavlidou, V., & Tassis, K. 2021, *A&A*, 656, A118
 Skalidis, R. & Tassis, K. 2021, *A&A*, 647, A186
 Wang, K., Testi, L., Ginsburg, A., et al. 2015, *mnras*, 450, 4043
 Ward-Thompson, D., Pattle, K., Bastien, P., et al. 2017, *apj*, 842, 66
 Wu, J., Qiu, K., Poidevin, F., et al. 2024, *ApJ*, 977, L31
 Zhao, M., Li, G.-X., & Qiu, K. 2024, *ApJ*, 976, 209
 Zhao, M., Li, G.-X., Xu, D., & Qiu, K. 2025, *arXiv e-prints*, arXiv:2508.01130

Appendix A: Data

Appendix A.1: Observations

The polarized data come from the B-fields In STar-forming Region Observations (BISTRO) survey (Ward-Thompson et al. 2017; Pattle et al. 2017). The resolution of the polarization data is 14'' (FWHM ~ 0.03 pc) measured by Scuba-2+POL-2 at 850 μ m. To calculate the polarized angle, the Stokes parameters Q and U are used in the equation:

$$\phi_p = 0.5 \times \arctan(U, Q), \quad (\text{A.1})$$

where polarized angle ϕ_p varies from -90° to 90° . This is the IAU convention. One has to use $\phi = 0.5 \times \arctan(-U, Q)$ to convert Planck measurement to this IAU convention. The magnetic field (after that, B-field) orientation can be obtained by adding 90° to the polarized angle: $\phi_B = \phi_p + 90^\circ$.

The H₂ column density map in the molecular cloud, OMC-1, comes from Herschel Gould Belt Survey¹ (Poglitsch et al. 2010; Griffin et al. 2010; Roy et al. 2013; Polychroni et al. 2013), which apply the SED fitting procedure (Wang et al. 2015) on the Herschel continuum at wavelengths of 70, 160, 250, 350, 500 μ m.

Appendix A.2: Simulations

The numerical simulation of molecular cloud selected in this work is identified within the three β_0 simulations applied by the constrained transport MHD option in Enzo (MHDCT) code (Collins et al. 2010; Burkhardt et al. 2015). The simulation conducted in this study analyzed the impact of self-gravity and magnetic fields on supersonic turbulence in isothermal molecular clouds, using high-resolution simulations and adaptive mesh refinement techniques. which detail in shown in (Collins et al. 2012; Burkhardt et al. 2015, 2020). The Enzo simulation with three dimensionless parameters provides us with massive information on physical processes:

$$\mathcal{M}_s = \frac{v_{\text{rms}}}{c_s} = 9 \quad (\text{A.2})$$

$$\alpha_{\text{vir}} = \frac{5v_{\text{rms}}^2}{3G\rho_0 L_0^2} = 1 \quad (\text{A.3})$$

$$\beta_0 = \frac{8\pi c_s^2 \rho_0}{B_0^2} = 0.2, 2, 20 \quad (\text{A.4})$$

where v_{rms} is the rms velocity fluctuation, c_s is sonic speed, ρ_0 is mean density, and B_0 is the mean magnetic field strength. With the same sonic Mach number \mathcal{M}_s and viral parameter α_{vir} in initial conditions, the difference only exists in initial magnetic pressure $\beta - 0$ with various B-field strength, The β_0 as 0.2, 2, and 20 present the strong B-field state, medium B-field, and weak B-field state. The clouds are in three different evolutionary stages started with self-gravity existing at $0.6t_{\text{ff}}$ (~ 0.76 Myr), where t_{ff} represents $1.1(n_H/10^3)^{-1/2}$ Myr (Collins et al. 2012; Burkhardt et al. 2015). Due to the short timescale of evolution, the gravitational collapse could barely affect the B- ρ relation in the simulation. The size of these molecular clouds is around 4.6^3 pc (256^3

pixels), with one-pixel size of approximately 0.018 pc (Burkhardt et al. 2015).

In this Enzo simulation, the thermal energy is located at the low state ($\mathcal{M}_s = 9$). Their timescale of evolution stage is 0.6 t_{ff} , around 0.76 Myr, which the timescale starts from when interstellar media collapse. Due to the short evolutionary time ($\sim 3.85 \times 10^{-21}$ g cm⁻³, or 821 cm⁻³), the gravitational energy less affects the system in simulation. With the similar mean density ρ_0 in these simulations, the different β_0 ($\sim 0.2, 2, 20$) present the different magnetic field states, strong B-field, stronger B-field (weaker than strong B-field but stronger than weak B-field), and weak B-field. The Alfvén Mach number \mathcal{M}_A in various simulations can be calculated by the energy ratio between the total magnetic energy E_B and kinetic energy E_k (Zhao et al. 2024):

$$\mathcal{M} = \sqrt{\frac{E_k}{E_B}} = \frac{\frac{1}{2}\rho\sigma_v^2}{B^2/8\pi} = \sqrt{4\pi\rho}\frac{\sigma_v}{B} \quad (\text{A.5})$$

where the \mathcal{M}_A in strong, medium, and weak magnetic field states can be estimated as 0.31, 0.49, and 1.29, respectively, when the simulation has evolved 0.6 t_{ff} .

Appendix B: Lorentz Force and Magnetic Tension in Enzo simulation

For this study, We use the simulation data ($\beta_0 = 20$, $t \approx 0.76$ Myr) on this work, whose the Alfvénic Mach number as 1.2 and the density range could be close to the actual molecular clouds (Zhao et al. 2024). This simulation setup is chosen such that the results resemble the structure of an actual star-forming molecular cloud, which is super-Alfvénic and close to the high-density molecular cloud (Zhao et al. 2024). The curvature mapping method can measure the Lorentz force in the pinch magnetic field, which mainly occurs in the high-density molecular cloud, and strong extra force, like self-gravity, distorts the local magnetic field. The Lorentz force ($f_L = \nabla \times \mathbf{B} \times \mathbf{B}/\mu_0$), magnetic tension ($f_t = \mathbf{B} \cdot \nabla \mathbf{B}/\mu_0$), and pressure $f_p = \nabla B^2/(2\mu_0)$ are measured in 3D space as Eq. 3 and Eq. 4. With the density increasing, Lorentz force stays at a similar value with the magnetic tension and pressure (See Fig. B.1). In the order of magnitude, the Lorentz force is comparable to the magnetic tension and pressure.

We compare the Lorentz force, magnetic tension, and magnetic pressure in 3D space (Collins et al. 2012; Burkhardt et al. 2015, 2020), where the similarity of two vectors, Lorentz force and another, is defined as:

$$D_{\text{similarity}} = \frac{\mathbf{v}_1 - \mathbf{v}_2}{\mathbf{v}_1 + \mathbf{v}_2} = \frac{f_L - f_{\text{torp}}}{f_L + -f_{\text{torp}}} \approx 0.5\theta_{\text{offset}} \quad (\text{B.1})$$

The similarity is close to the half of the offset angle between two vectors in geometry (see Fig. 1) The similarity and offset angle in the 2D plane (POS) will be needed in actual observation. The offset angle in 3D space has a different probability density (see Ap. C). To accurately obtain the offset angle, the distribution of the offset angle is weighted by the probability density function (see Ap. C). The offset angle between magnetic tension and Lorentz force in the 2D plane (similar to the POS) is around 11° , and they have similar sizes (see Fig. B.2). The offset angle between magnetic pressure and Lorentz force in the 2D plane (similar to the POS) is around 19° (see Fig. B.2), which are also close to parallel (offset angle $< 30^\circ$). The magnetic tension and pressure resemble the Lorentz force in both magnitude and orientation.

¹ http://www.herschel.fr/cea/gouldbelt/en/Phocea/Vie_des_labos/Ast/ast_visu.php?id_ast=66

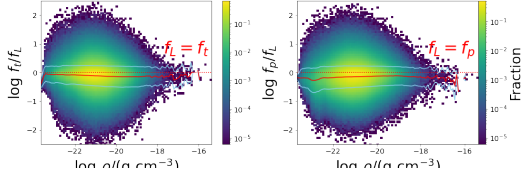


Fig. B.1. Distribution of the ratio between Lorentz Force and Magnetic Tension, Magnetic Pressure in Enzo simulations. This panel presents a 2D histogram between the ratio of Lorentz Force and magnetic tension, magnetic pressure, whose intensity is shown at the log scale. The red line presents the mean value of the ratio between Lorentz Force and magnetic tension at each density range. The blue lines indicate the distribution range, approximately equal to $\sqrt{8 \ln 2}$ times the standard deviation (σ) fitted by Gaussian distribution, which corresponds to the full width at half maximum (FWHM). The red dotted line shows the $f_L/f_L = 1$. The dispersion range shows the error range, around half the order of magnitudes.

Appendix C: Remove the projection effect in probability density distributions

The probability density function, $p(\theta)$, of the angle between two vectors of random distribution is distributed in an N-dimensional space as:

$$p(\theta) = \frac{\Gamma(\frac{n}{2})}{\Gamma(\frac{n-1}{2})} \frac{\sin^{n-2}(\theta)}{\sqrt{\pi}} \quad (\text{C.1})$$

where n is the number of dimensions, and θ is the angle between two vectors of random distribution.

In 3-dimension space, the probability density function of angle $p(\theta)$ is

$$p(\theta) = \frac{1}{2} \sin \theta \quad (\text{C.2})$$

To remove the projection effect, we use the probability density function $p(\theta)$ to weight the angle distribution:

$$P(\theta_{\text{corrected}}) = P(\theta_{\text{original}})/p(\theta) \quad (\text{C.3})$$

where θ_{original} represents the original angle distribution and $\theta_{\text{corrected}}$ represents the corrected angle distribution, with the projected effects removed.

Appendix D: Estimate Distribution of Magnetic Field Strength

Accurately measuring the distribution of magnetic field strength on POS is challenging due to limitations in existing methods, such as Zeeman splitting (Crutcher et al. 2010) and the Davis-Chandrasekhar-Fermi (DCF) method (Davis 1951; Chandrasekhar & Fermi 1953; Crutcher et al. 2004). Zeeman splitting hardly maps magnetic field strength effectively which observations usually come from a single point source due to a low signal-to-noise ratio. The DCF method ($B_{\text{pos}} = 0.5 \sqrt{4\pi} \sigma_v / \sigma_\phi$) relies on the assumption of equipartition between turbulent and magnetic energy and turbulence cause the distortion of straight magnetic field line, introducing errors from various observational uncertainties such as density (ρ) derived from continuum data (Zhao et al. 2025), velocity dispersion (σ_v), and magnetic field orientation angle dispersion (σ_ϕ) derived from polarization measurements. The DCF combined with the Autocorrelation Function

(ACF, (Houde et al. 2009, 2016)) effectively avoids the overestimation of magnetic field distortion from turbulence but only provides one value of magnetic field strength in single clouds.

To measure the scale of POS Lorentz force, we choose the ST method (Skalidis & Tassis 2021; Arzoumanian et al. 2021) to estimate the plane distribution of magnetic field strength:

$$B_{\text{pos}} = \sqrt{2\pi} \rho \frac{\sigma_v}{\sqrt{\sigma_\phi}} \quad (\text{D.1})$$

where the ρ is the density of ISM, the σ_v as velocity dispersion relates to turbulence, σ_ϕ is the magnetic field orientation angle dispersion which is affected by small-scale turbulence. The assumption of ST method (Skalidis & Tassis 2021; Arzoumanian et al. 2021) is similar to the DCF method (Davis 1951; Chandrasekhar & Fermi 1953; Crutcher et al. 2004). Different occur in the handle of angle dispersion σ_ϕ , where that in ST method is $\sigma_\phi^{-0.5}$ and in DCF method is σ_ϕ^{-1} (DCF method : $B_{\text{pos}} = Q \sqrt{4\pi} \rho \frac{\sigma_v}{\sigma_\phi}$). Regarding error propagation, the ST method could reduce the error from angle dispersion to magnetic field strength compared to the DCF method. Thus, we use the ST to estimate the plane distribution of magnetic field strength in OMC-1.

As Fig. C.1 shows, we calculate the basic parameters, density ρ , non-thermal velocity dispersion $\sigma_{v,NT}$, and magnetic field orientation angle dispersion in the same scale ($\sim 40''$, 0.07 pc). The volume density comes from the column density observed by Herschel (Poglitsch et al. 2010; Griffin et al. 2010; Roy et al. 2013; Polychroni et al. 2013) (see Ap. A), using the Constrained Diffusion Method (Li 2022) and its derivative method (Zhao & Li +, in prep.) The angle dispersion is calculated by magnetic field orientation derived by $850\mu\text{m}$ dust polarization (Pattle et al. 2017) and mapped by the sub-block of 3×3 beams (Zhao & Li +, in prep.). The non-thermal velocity dispersion comes from the velocity dispersion and kinetic temperature of NH_3 observed by GBT (Friesen et al. 2017).

The distribution of total magnetic field strength in OMC-1 is estimated by POS component of magnetic field strength (Crutcher et al. 2004):

$$B_{\text{tot}} = \frac{4}{\pi} B_{\text{pos}} \quad (\text{D.2})$$

The distribution is shown in Fig. C.1

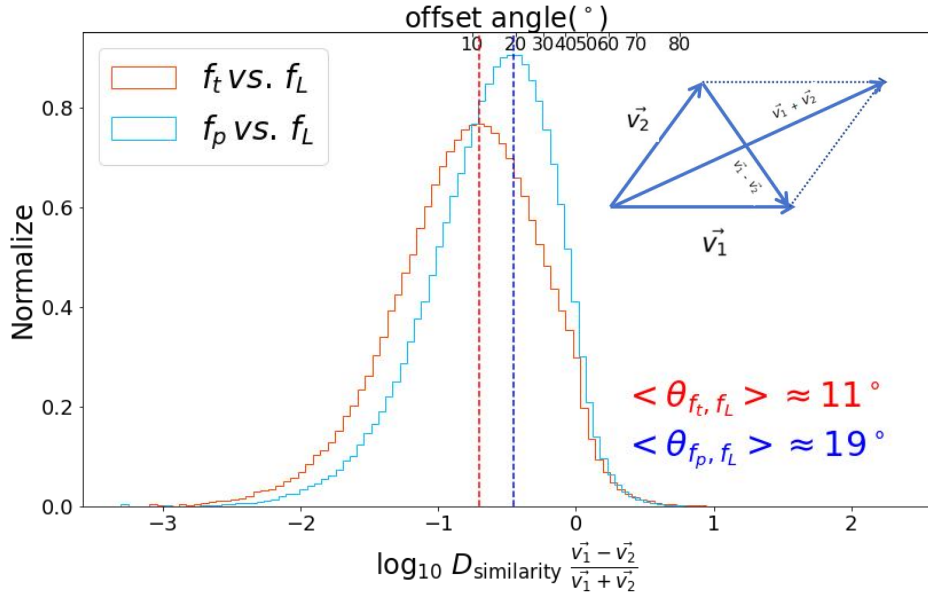


Fig. B.2. Distribution of similarity and offset angle between Lorentz force and magnetic tension, magnetic pressure. By projecting from 3D space to the 2D plane, magnetic tension, or magnetic pressure, \vec{V}_1 is close to Lorentz force \vec{V}_2 , whose offset angle between magnetic tension/pressure and Lorentz force is around 11° , 19° , respectively. The canton in the top right corner displays the similarity of two vectors. The Lorentz force is similar to the magnetic tension and pressure in order.

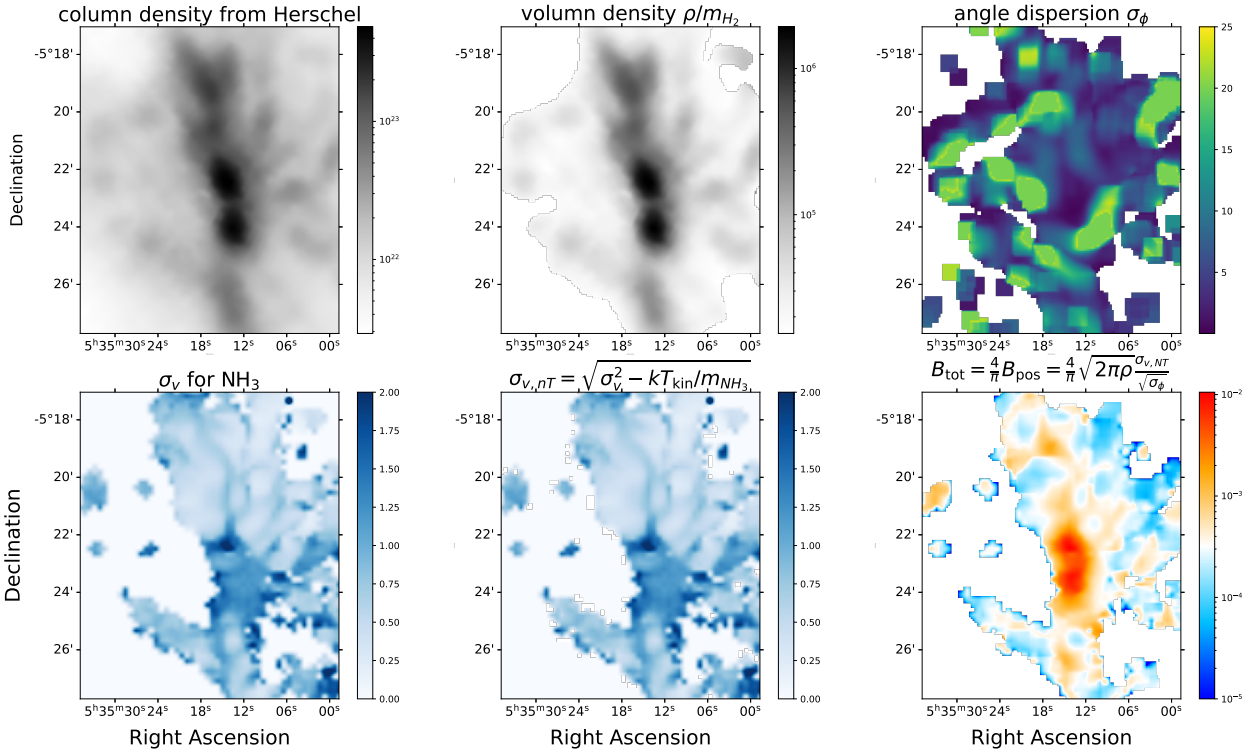


Fig. C.1. Estimate the magnetic field strength distribution. We use the ST method to estimate the magnetic field strength. These panels present the distribution of column density, volume density,